



King Saud University
Arabian Journal of Chemistry

www.ksu.edu.sa
www.sciencedirect.com



ORIGINAL ARTICLE

Synthesis, thermal property and antifungal evaluation of pyrazine esters



Fangyao Su ^a, Zhengyu Su ^a, Qianrui Zhao ^a, Zhe Zhao ^b, Zhiyong Wu ^a,
Mingqin Zhao ^{a,*}, Miao Lai ^{a,*}

^a Flavors and Fragrance Engineering & Technology Research Center of Henan Province, College of Tobacco Science, Henan Agricultural University, Zhengzhou 450002, China

^b Jinan Cigarette Factory of China Tobacco Shandong Industrial Co. Ltd., Jinan 250104, China

Received 8 August 2022; accepted 9 October 2022

Available online 13 October 2022

KEYWORDS

Pyrazine esters;
Organoleptic characteristics;
Thermal behaviors;
Antifungal activities

Abstract Synthesis, thermal properties, as well as antifungal assessment of pyrazine esters were handed in this work. The metal-free esterification of pyrazinyl methanol and acid chloride derivatives in a stoichiometric ratio yielded the following compounds: pyrazin-2-ylmethyl benzoate (**3a**), (5-methylpyrazin-2-yl) methyl benzoate (**3b**), 1-(pyrazin-2-yl) ethyl benzoate (**3c**), 2-(pyrazin-2-yl) ethyl benzoate (**3d**), pyrazin-2-ylmethyl pivalate (**3e**). The spectral results totally showed that the synthesis conditions used permitted the compounds to be produced with great yield. The characterization included ¹H NMR, ¹³C NMR, IR, HRMS and organoleptic tests. Their thermal degradation process was examined by using the TG (thermogravimetry) and DSC (differential scanning calorimeter) methods. The pyrolysis products of the pyrazine esters in inert and oxidative atmospheres were analyzed by the Py-GC/MS (pyrolysis–gas chromatography/mass spectrometry) method. It revealed that **3a–3e** were totally evaporated throughout the pyrolysis experiments at low temperatures. And they evaporated with high relative contents in pure nitrogen (86.12%–94.17%) and oxidative (75.01%–88.85%) atmospheres, with only a small amount decomposing into a series of substances. Additionally, the *in vitro* antifungal effects of compounds **3a–3e** against *R. solani*, *P. nicotianae*, *F. oxysporum*, *F. graminearum*, and *F. moniliforme* were further investigated using the mycelial growth rate methodology. The findings shown that compound **3c** has 94% and 80% inhibitor rates at 0.5 mg/ml against *R. solani* and *P. nicotianae*, respectively, with an EC₅₀ value (half maximum effective concentration) of 0.0191 mg/ml and 0.1870 mg/ml, respectively.

* Corresponding authors.

E-mail addresses: zhaomingqin@126.com (M. Zhao), laimiao@henau.edu.cn (M. Lai).

Peer review under responsibility of King Saud University.



<https://doi.org/10.1016/j.arabjc.2022.104351>

1878-5352 © 2022 The Author(s). Published by Elsevier B.V. on behalf of King Saud University.

This is an open access article under the CC BY-NC-ND license (<http://creativecommons.org/licenses/by-nc-nd/4.0/>).

Similarly, that of compounds **3a** and **3b** exhibited 82% and 91% at 0.5 mg/ml against *R. solani*, with an EC₅₀ value of 0.0209 mg/ml and 0.0218 mg/ml, respectively. The molecular docking of compound **3c** with SDH (Succinate dehydrogenase) was preliminarily performed to reveal the binding modes in active pocket and analyze the interactions between the molecules and the protein.

© 2022 The Author(s). Published by Elsevier B.V. on behalf of King Saud University. This is an open access article under the CC BY-NC-ND license (<http://creativecommons.org/licenses/by-nc-nd/4.0/>).

1. Introduction

Pyrazines are by far the most commonly distributed aromatic hydrocarbons, which are prominent in the organic chemistry area due to their versatile uses. They are almost ubiquitous in a wide variety of natural products [Kosuge and Kamiya, 1962; Bohman et al., 2012], bioactive molecules [Juhás and Zitko, 2020; Asaki et al., 2007], drugs [Tambat et al., 2022; Chylewska et al., 2019], agrochemicals [Fales et al., 1988; Oldham and Morgan, 1993], dyes [Lee et al., 2020; Al-Hazmy et al., 1999], and flavors [Mortzfeld et al., 2020; Michael et al., 2005; Masuda et al., 1981]. Pyrazine derivatives also aroused the interest of the food additive and flavoring substance industries in recent decades due to their unique aromatic organoleptic properties at very low concentrations [Wagner et al., 1999; Koehler et al., 1971]. Because pyrazine metabolism produces innocuous products, they were deemed safe and can be utilized as GRAS flavor additives [Adams et al., 2002]. Pyrazine derivatives can be found naturally in potatoes, coffee beans, cocoa beans, nuts, beef, and tobacco [Dolezal and Zitko, 2015; Maga et al., 1973] with applications in numerous areas. For example, they can be used as flavor additives to enhance the aroma of toast, peanut products, meat, coffee, cocoa products and tobacco due to their nutty, roasted, green bell pepper, and popcorn-like odor [Mihara and Masuda, 1988; Maga and Katz, 1982; Krems and Spoerri, 1947]. Plus, these pyrazine derivatives also continue to attract the attention of several investigators due to their diverse biological applications like antimicrobial [Bonde and Gaikwad, 2004], antifungal [Kucerova-Chlupacova et al., 2015], antimycobacterial [Seitz et al., 2002], antiviral [Seliem et al., 2021], antiinflammatory [Da Silva et al., 2010], anticancer [Rolver et al., 2020] and so forth. Thus, there has been a growing interest in creating novel, sustainable, one-pot synthetic strategies for preparing pyrazine derivatives in recent years. In the last decade, pyrazine esters have usually been available with transition metals catalyzed by the method of C—H bond activation [Cheng et al., 2019; Eisele et al., 2019; Chen et al., 2018], C—C bond activation [Huang et al., 2014; Peng et al., 2016; Prasad et al., 2005], and C—N bond activation [Chen et al., 2020; Jaiswal et al., 2018], respectively. Since many of these methodologies require harsh reaction conditions, often involve metal catalysts and lack of step efficiency, we report here a new method for their synthesis based on the catalyst-free esterification of pyrazine methanols with acyl chlorides in an air atmosphere with characterization using different spectral techniques including NMR, IR, and HRMS.

It is well known that the formation mechanism and thermal decomposition of pyrazines are highly correlated to the Maillard reaction [Koehler and Odell, 1970], which formed during thermal treatments by the condensation of a reducing carbohydrate with an amino component and provides a unique flavor as well as browning-reaction to processed products [Amrani-Hemaimi et al., 1995]. Investigating their organoleptic properties as well as stability and heated decomposition products is therefore essential. The organoleptic properties were evaluated based on odor and appearance. TG, DSC and Py-GC/MS are useful experimental techniques which commonly used in thermal analysis [Lai et al., 2017; Czégény et al., 2016; Xie et al., 2007].

Moreover, previous research has demonstrated that pyrazines have numerous pharmacological effects, with the majority of them focusing on the discovery of novel medications and therapeutic targets. [Lee et al., 2022; Zhu et al., 2020; Miniyar et al., 2013]. However, they have the lack of a further study of influence of the pyrazine moiety for inhibitory effects on fungal. It is noting that the infections of *Fusarium graminearum*, *Fusarium oxysporum*, *Fusarium moniliforme*, *Phytophthora nicotianae* and *Rhizoctonia solani* are the well-known causative agents of bacterial blight infections of wheat, maize, and tobacco in economically important crops [Harries et al., 2020; Yang et al., 2017; Ntushelo, 2016; Gonzalez et al., 2011; Murillo et al., 1998; Nelson, 1992] which colonized in different plant tissues, such as stems, leaf, and flowers, and then ingested nutrients off host cells, causing severe defoliation and a decrease in crops production [Wang et al., 2016]. Therefore, research on pyrazine derivatives aimed at the development of antifungal agents for these diseases is important in agricultural crops.

In this research, we demonstrate the synthesis, characterization, and thermal characteristics of pyrazine ester derivatives, as well as experiments into the compounds' inhibitory effects on fungal growth. The organoleptic profiles, including odor and color properties of the synthesized pyrazine ester derivatives were evaluated. The thermal stability of the compounds was investigated in N₂ atmosphere by means of TG and DSC. And the qualitative and quantitative assessment of pyrolysis products was performed on-line with Py-GCMS. Furthermore, we assessed the antifungal activities of pyrazine esters against *R. solani*, *P. nicotianae*, *F. oxysporum*, *F. graminearum*, and *F. moniliforme*. And we also have preliminarily explored the possible antifungal mechanism of synthesized target compounds by molecular docking.

2. Materials and methods

2.1. Chemicals and instruments

The identities of the chemical reagents used in this paper are listed in Table 1. Five crop-threatening pathogenic fungi (*R. solani*, *P. nicotianae*, *F. oxysporum*, *F. graminearum*, and *F. moniliforme*) were obtained from College of Tobacco Science in Henan Agricultural University. The analytical reagents (AR) with satisfactory standards were bought from Tianjin Damao Technology Co., Ltd. (China).

The ¹H (400 MHz) and ¹³C (100 MHz) NMR spectra were collected at room temperature using a BRUKER AVANCE III 400 MHz spectromete, CDCl₃ as the solvent, and tetramethylsilane (TMS) as the internal standard. The FT-IR spectra of the KBr micropellet extract was determined using a Perkin Elmer spectrum 100 Fourier transform infrared spectrometer. HRMS measurements were taken using an AB SCIEX Triple TOF 5600 + high resolution mass spectrometer (USA)

2.1.1. Preparation of compounds **3a–3e**

The 2-pyrazinylmethanol (0.4 mmol, 2.0 eq) and Et₃N (2.5 mmol, 0.35 ml) were dissolved in CH₂Cl₂ (6 ml) with an

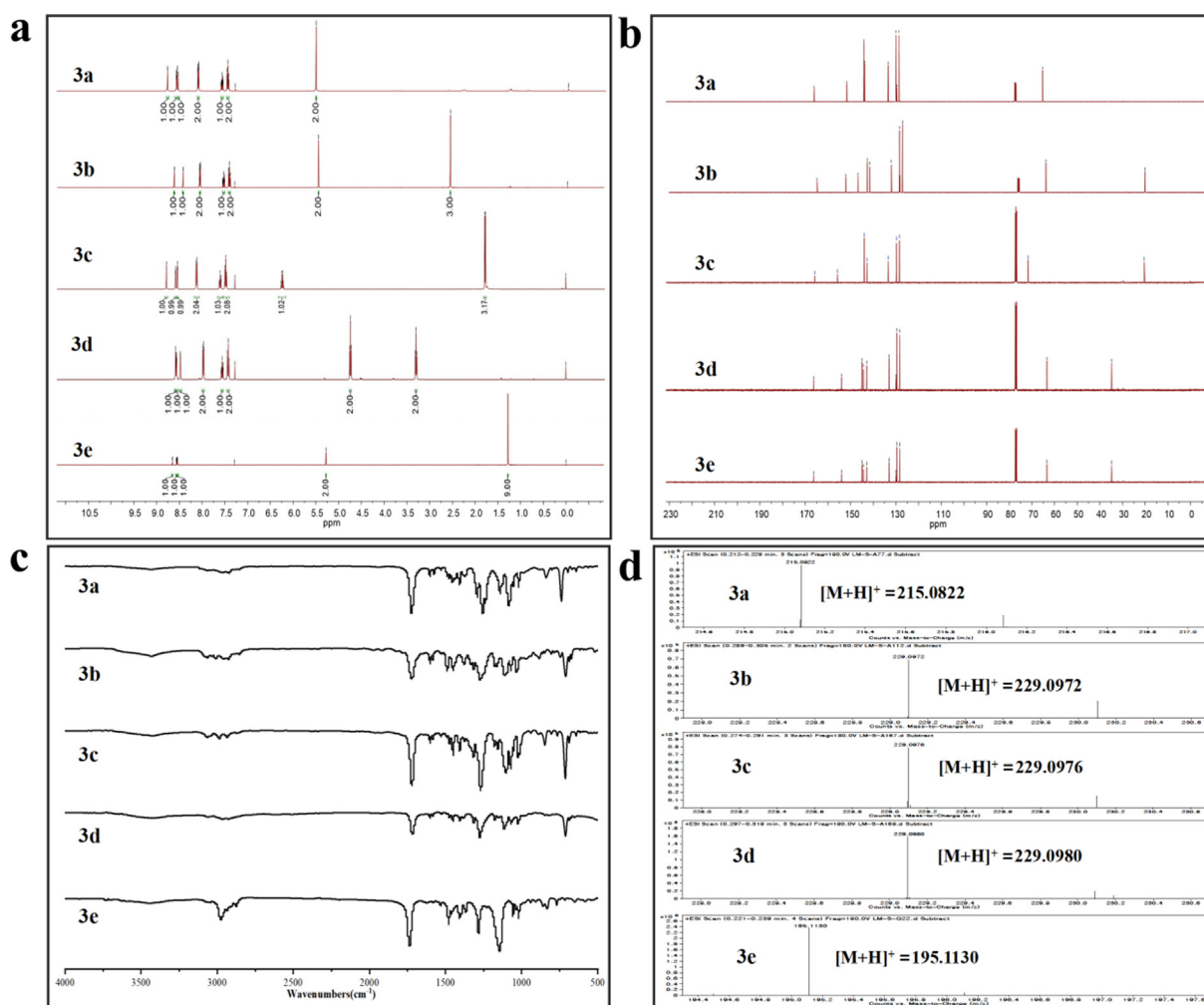


Fig. 1 ^1H NMR (a), ^{13}C NMR (b), IR (c) and HRMS (d) of **3a-3e**.

Table 1 The informations of the chemical reagents.

No.	Chemical name	CAS Number	Structures	Purchase company	Purity
1	2-pyrazinylmethanol	6705-33-5		Shanghai Macklin Biochemical Co., Ltd. (China)	97%
2	1-(2-pyrazinyl)-1-ethanol	94777-52-3		Shanghai Macklin Biochemical Co., Ltd. (China)	95%
3	5-methyl-2-pyrazinemethanol	61892-95-3		Shanghai Macklin Biochemical Co., Ltd. (China)	98%
4	2-pyrazinylethyl alcohol	6705-31-3		Shanghai Macklin Biochemical Co., Ltd. (China)	97%
5	benzoyl chloride	98-88-4		Shanghai Macklin Biochemical Co., Ltd. (China)	99%
6	pivaloyl chloride	3282-30-2		Shanghai Macklin Biochemical Co., Ltd. (China)	98%

ice bath, then acid chlorides (0.2 mmol, 1.0 eq) was added drop by drop and stirred for 2 min. The ice bath was withdrawn after 20 min of churning, and the stirring was continued for 12 h at 140 °C in air environment. After the mixture cooled to room temperature, it was quenched with 1 N HCl, and

diluted with 3 × 5 ml CH_2Cl_2 . The mixed extract was progressively washed with brine and saturated NaHCO_3 , dried over by anhydrous Na_2SO_4 , filtered and concentrated in vacuo. Finally, the residue was purified using silica gel flash column chromatography to get the pure product **3a**.

The preparation of compounds **3b–3e** was the same as compound **3a**.

2.1.2. Structures data

2.1.2.1. Pyrazin-2-ylmethyl benzoate (3a). Eluent: *n*-pentane/EtOAc = 7/1; ¹H NMR (400 MHz, CDCl₃) ppm: 8.78 (d, *J* = 1.1 Hz, 1H), 8.62 – 8.57 (m, 1H), 8.56 (d, *J* = 2.5 Hz, 1H), 8.13 – 8.09 (m, 2H), 7.61 – 7.56 (m, 1H), 7.48 – 7.44 (m, 2H), 5.53 (s, 2H); ¹³C NMR (100 MHz, CDCl₃) ppm: 166.01, 151.57, 144.14, 143.72, 133.40, 129.80, 129.41, 128.50, 65.13; IR (KBr) ν_{\max} 3434, 2855, 1723, 1457, 1292, 1257, 1055, 838, and 738 cm⁻¹; HRMS (ESI) calcd. for C₁₂H₁₀N₂O₂: [M + H]⁺: 215.0821, found: 215.0822.

2.1.2.2. (5-Methylpyrazin-2-yl) methyl benzoate (3b). Eluent: *n*-pentane/EtOAc = 5/1; ¹H NMR (400 MHz, CDCl₃) ppm: 8.77 (d, *J* = 1.2 Hz, 1H), 8.60 – 8.55 (m, 1H), 8.53 (d, *J* = 2.5 Hz, 1H), 8.14 – 8.08 (m, 2H), 7.62 – 7.56 (m, 1H), 7.47 (t, *J* = 7.7 Hz, 2H), 6.23 (q, *J* = 6.7 Hz, 1H), 1.77 (d, *J* = 6.7 Hz, 3H); ¹³C NMR (100 MHz, CDCl₃) ppm: 165.72, 155.80, 143.96, 142.70, 133.32, 129.77, 128.48, 71.73, 20.39; IR (KBr) ν_{\max} 3062, 2985, 2935, 1720, 1601, 1584, 1269, 1099, 712 cm⁻¹; HRMS (ESI) calcd. for C₁₃H₁₂N₂O₂: [M + H]⁺: 229.0977, found: 229.0976.

2.1.2.3. 1-(Pyrazin-2-yl) ethyl benzoate (3c). Eluent: *n*-pentane/EtOAc = 5/1; ¹H NMR (400 MHz, CDCl₃) ppm: 8.77 (d, *J* = 1.2 Hz, 1H), 8.60 – 8.55 (m, 1H), 8.53 (d, *J* = 2.5 Hz, 1H), 8.14 – 8.08 (m, 2H), 7.62 – 7.56 (m, 1H), 7.47 (t, *J* = 7.7 Hz, 2H), 6.23 (q, *J* = 6.7 Hz, 1H), 1.77 (d, *J* = 6.7 Hz, 3H); ¹³C NMR (100 MHz, CDCl₃) ppm: 165.72, 155.80, 143.96, 142.70, 133.32, 129.77, 128.48, 71.73, 20.39; IR (KBr) ν_{\max} 3062, 2985, 2935, 1720, 1601, 1584, 1269, 1099, 712 cm⁻¹; HRMS (ESI) calcd. for C₁₃H₁₂N₂O₂: [M + H]⁺: 229.0977, found: 229.0976.

2.1.2.4. 2-(Pyrazin-2-yl) ethyl benzoate (3d). Eluent: *n*-pentane/EtOAc = 3/1; ¹H NMR (400 MHz, CDCl₃) ppm: 8.57 (s, 1H), 8.56 – 8.52 (m, 1H), 8.46 (d, *J* = 2.4 Hz, 1H), 7.99 – 7.94 (m, 2H), 7.57 – 7.52 (m, 1H), 7.41 (t, *J* = 7.7 Hz, 2H), 4.73 (t, *J* = 6.5 Hz, 2H), 3.29 (t, *J* = 6.5 Hz, 2H); ¹³C NMR (100 MHz, CDCl₃) ppm: 166.35, 154.00, 145.02, 144.36, 142.90, 133.07, 129.93, 129.54, 128.40, 63.38, 34.79; IR (KBr) ν_{\max} 3061, 2966, 2925, 1717, 1602, 1583, 1274, 1113, 711 cm⁻¹; HRMS (ESI) calcd. for C₁₃H₁₂N₂O₂: [M + H]⁺: 229.0977, found: 229.0980.

2.1.2.5. Pyrazin-2-ylmethyl pivalate (3e). Eluent: *n*-pentane/EtOAc = 7/1; ¹H NMR (400 MHz, CDCl₃) ppm: 8.68 – 8.64 (m, 1H), 8.58 – 8.55 (m, 1H), 8.54 (d, *J* = 2.5 Hz, 1H), 5.28 (s, 2H), 1.28 (s, 9H); ¹³C NMR (100 MHz, CDCl₃) ppm: 177.94, 151.95, 144.03, 143.91, 143.30, 64.66, 38.86, 27.16; IR (KBr) ν_{\max} 2975, 2936, 2874, 1736, 1480, 1283, 1144, 1018, and 832 cm⁻¹; HRMS (ESI) calcd. for C₁₀H₁₄N₂O₂: [M + H]⁺: 195.1134, found: 195.1130.

2.2. Organoleptic testing

The organoleptic testing used parameters including odor and appearance. The evaluations were conducted in a sensory room, the temperature was controlled at 21 ± 1 °C, and air

humidity was controlled at 50%~55%. All compounds were evaluated for their odor and color by a panel of experts from the Flavors and Fragrance Engineering and Technology Research Center of Henan Province. The organoleptic properties were based on a triangular test which was performed using one test sample and two blank samples (ion-exchanged water) and evaluated for orthonasal aroma by using undiluted samples. Each expert sniffed the samples, and they were asked to write down the types of odours and appearance properties detected on the evaluation sheet. This test was repeated at least three times. All experts agreed on the identified profile.

2.3. TG and DSC method

TG-DSC analysis were carried out on a Germany Netzsch STA 449 PC simultaneous thermal analyzer under the following operational conditions: spectral purity Al₂O₃ crucible, constant heating rate of 10 °C min⁻¹, a dynamic carrier gas of helium (60 ml min⁻¹), a temperature range of 30–550 °C, and a sample mass of 10 mg. The TG, DTG, and DSC curves were all acquired at the same time.

2.4. Py-GC/MS method

The Pyroprobe 5250 T (CDS, Analytical Inc.) was utilized in conjunction with the GC/MS (Agilent, 7890A/5975C). Approximately 1 mg of material was placed in a quartz tube (25 mm) that was nominally heated at the rate of 30 °C ms⁻¹ and pyrolyzed for 20 s at 100–300, 300–900, and 30–900 °C, respectively.

The chromatographic separation was carried out on the Agilent DB-5MS fusing with silica capillary column (60 m × 250 μm × 0.25 μm). The injection system's temperature was controlled at 300 °C. The oven temperature was initially set to 50 °C at the start and quickly increased to 80 °C (6 °C min⁻¹), then to 110 °C (4 °C min⁻¹) for 2 min, finally lastly to 250 °C (5 °C min⁻¹) for 2 min. The carrier gas (Helium) flow was constant at 1 ml min⁻¹ and the split ratio was 50:1. The mass spectrometer was used to examine the separated substances. The ionization energy of EI was 70 eV, and the temperature of transfer line was 300 °C. The quadrupole was set at 150 °C while the ion source was at 230 °C. The mass spectra included a solvent delay of 3.1 min and ranged from *m/z* 30 to 500.

2.5. In vitro antifungal method

The *in vitro* antifungal effectiveness of compounds **3a–3e** against five fungus strains (*R. solani*, *P. nicotianae*, *F. oxysporum*, *F. graminearum*, and *F. moniliforme*) were evaluated by the mycelial growth rate method (Yang et al., 2021; Bao et al., 2019) at a concentration of 0.5 mg/ml, using triazolone (0.03 mg/ml) as the standard drug. After adjusting the final chemical concentration in the medium, the fungal mycelium was transferred to the test plate and cultivated for 3–7 days at 25 °C. The radial growth of fungal colonies was measured on the 4–8 day. Each experiment was being performed three times. The EC₅₀ (half maximal effective concentration) values of each compound were calculated statistically by Probit analysis with the SPSS 17.0 software.

2.6. Molecular docking methods

The molecular docking in this paper was performed by Auto-Dock Vina (Vina, version 1.1.2). The structure and sequence of target protein (Succinate dehydrogenase, SDH: Q9UTJ7) were retrieved from the Protein Data Bank (PDB) RCSB (<https://www.pdb.org/>) and the structure of compound **3c** was downloaded from the Pubchem database (<https://pubchem.ncbi.nlm.nih.gov/>). The PyMOL (version 4.3.0) software (<https://pymol.org/>) was used to separate the original ligand and protein structures, dehydrate them, and eliminate the organics. The AutodockTools (<https://mglttools.scripps.edu/downloads>) were used to: build protein structures; verify charges; adjust atom kinds; dock grid boxes for hydrogenation; and determine the root of the chemical composition (compound **3c**). The scores for the combination of compound **3c** with SDH (Q9UTJ7) were calculated after docking with Vina. The PLIP online platform were used for display and analysis of the findings of acting force in 3D angles.

3. Results and discussion

3.1. Synthesis and identification

We successfully synthesized the title compounds **3a-3e** using the metal-free, and one-pot method. As shown in [Scheme 1](#), they were subjected to the conventional reaction conditions and afforded with good yields (79%–90%). And the structures of these synthesized compounds were confirmed by spectral data, such as ^1H NMR, ^{13}C NMR, IR and HRMS.

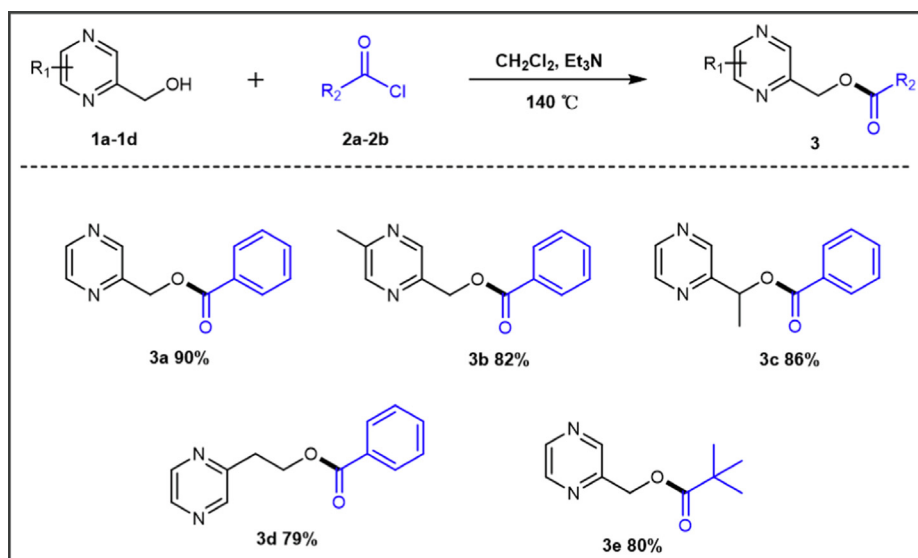
The resonance signals in ^1H NMR are clearly visible in [Fig. 1\(a\)](#) for the protons assigned to carbon-carbon double bonds in pyrazine esters structures: $\delta = 8.78\text{--}8.16$ ppm (pyrazine) and $\delta = 8.11\text{--}7.41$ ppm (benzene ring). For the alkoxy groups of compounds, protons were detected in the range of 3.20–6.27 and 1.22–2.75 ppm. Furthermore, the protons indicative of *tert*-amyl groups derived from pivaloyl chloride were identified at $\delta = 1.28$ ppm. Compounds **3a-3e** exhibited

typical carbon peaks between 128 and 133 ppm ascribed to the pyrazine rings, and the carbonyl carbon peak was observed at about 166 ppm in ^{13}C NMR of [Fig. 1](#) (b). In addition, [Fig. 1](#) (c) showed the IR spectra of the obtained pyrazine esters. The emergence of stretching vibrations of carbonyl groups in esters at around 1735 cm^{-1} was clearly observed. It was clearly stated that the lack of the absorption signals characteristic for stretching vibrations of alcoholic hydroxyl groups was the stretching vibrations of C–O bonds for esters with the appearance in the range of $1269\text{--}1283\text{ cm}^{-1}$. Meanwhile, a new distinctive absorption peak in the region of $671\text{--}674\text{ cm}^{-1}$ appeared, indicating that the phenyl group was effectively coupled (**3a-3d**). The stretching vibrations of *tert*-amyl groups emerged in **3e** at 1397 and 1407 cm^{-1} . Furthermore, positive ionization mass spectrometry in [Fig. 1](#) (d) revealed that all compounds had the molecular-ion peak $[\text{M} + \text{H}]^+$ and matched the estimated values. In summary, it confirmed that the functional groups were completely consumed throughout the esterification process and produced the formation of the desirable products. All of the spectra verified the formation with the anticipated structure, as expected.

As shown in [Scheme 2](#), to further assess the superior scalability of this established method, a large scale (7 mmol) of experiments were carried out between pyrazine methanols (**1a-1d**) and acyl chlorides (**2a-2b**), which delivered the desired products **3a**, **3b**, and **3c** with an excellent yield of 85% (1.27 g), 80% (1.28 g), and 82% (1.31 g), respectively. And the reactions of 2-pyrazinylethyl alcohol (**1d**), 2-pyrazine methanol (**1a**) with benzoyl chloride (**2a**) and pivaloyl chloride (**2b**) could also smoothly afford the esterification products in good yields (**3d-3e**, 72%–78%).

3.2. Organoleptic characteristics

The appearance properties were evaluated by a panel of experts, and [Table 2](#) summarized the main notes for **3a-3e**. Note that the compounds shared a number of similarities in odour properties with each other as well as some important



Scheme 1 Synthesis route of the target compounds **3a-3e**.

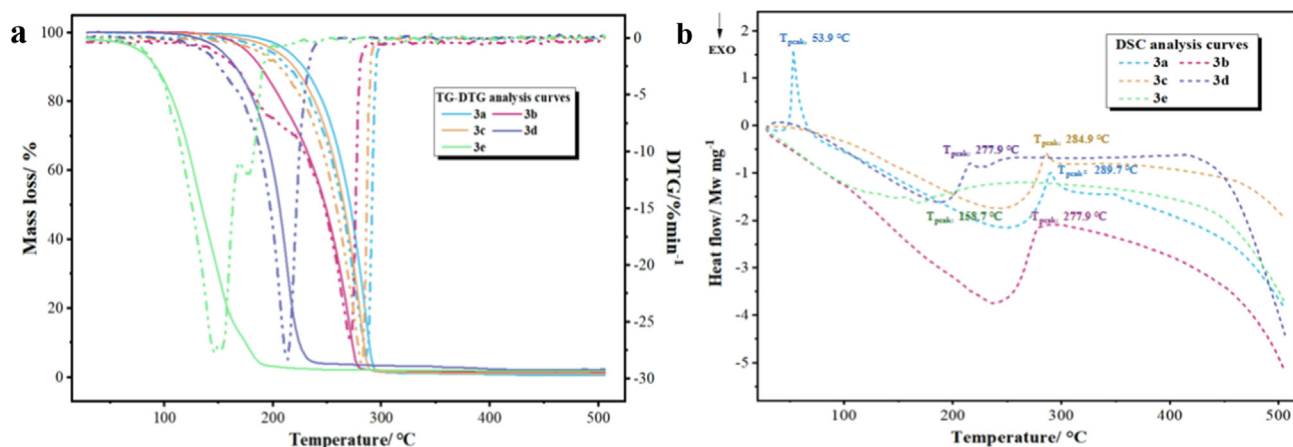
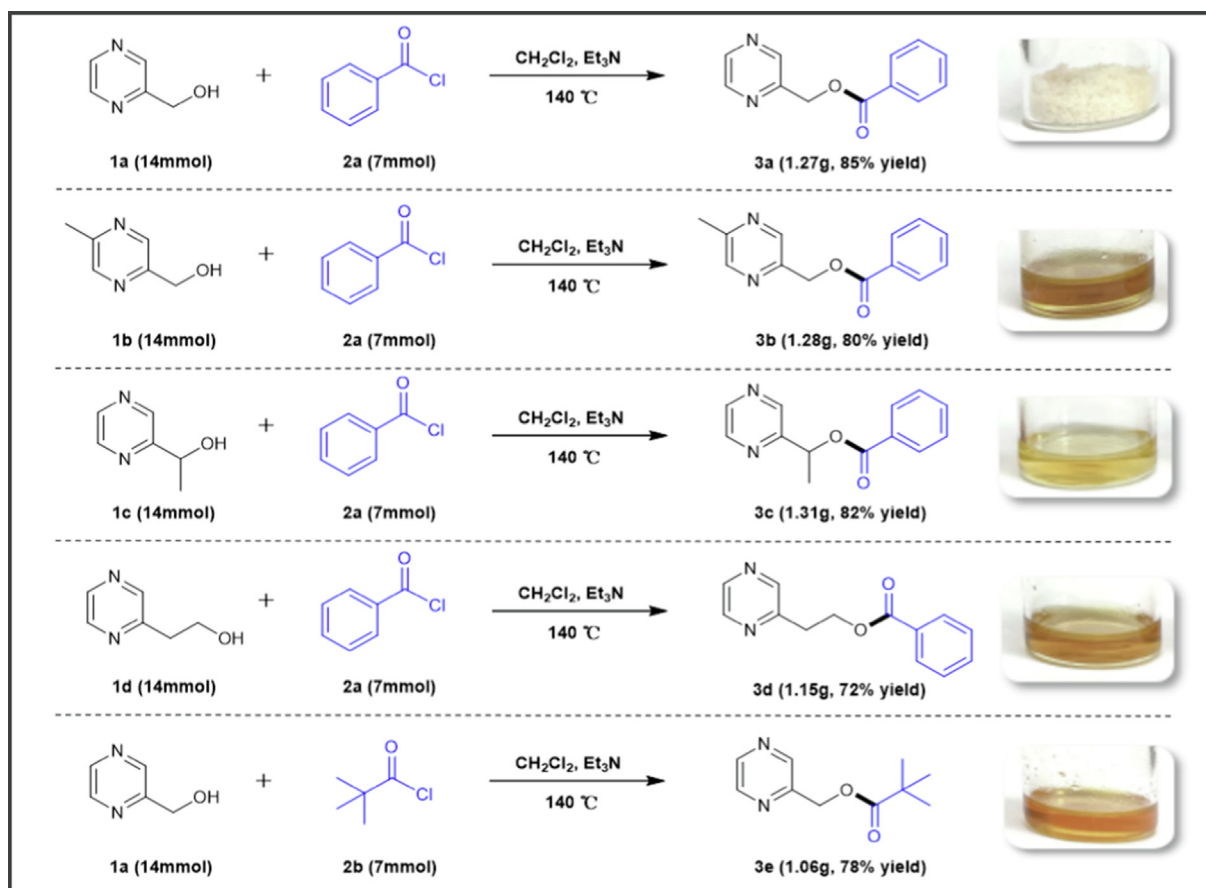


Fig. 2 TG-DTG curves of 3a-3e (a), DSC curves of 3a-3e (b).



Scheme 2 Gram-scale reactions to obtain the compounds 3a-3e.

differences. For instance, all the compounds possessed woody or green notes and showed gourmand tonalities, which could be linked to the common flavors found in most pyrazine derivatives. The odour intensity of 3a was lower than that of 3b, 3b was lower than that of 3e, 3e was lower than that of 3c, and 3d had the weakest odour intensity of all compounds. Besides, compound 3c had a high and intensive popcorn-like and cocoa aroma with better long-lastingness, could release and imitate the food flavor commendably.

3.3. Thermal analysis

The TG, DTG, and DSC curves of the title compounds during 30–550 °C at the heating rate of 10 °C min⁻¹ were obtained in Fig. 2.

As shown in Fig. 2 (a), the decomposition of compounds 3a, 3b, and 3c occurred at temperatures ranging from 183.4 to 290.4, 160.9 to 295.4, and 153.1 to 295.4 °C, respectively. And it reveals that the maximum decomposition rate of

Table 2 Organoleptic profile of compounds **3a-3e**.

Sample	Organoleptic profile	
	Appearance	Odor
3a	Linen; Powder	Weak, woody, pine, a bit of green pepper
3b	Sienna; Liquid	Roasted, cocoa, earthy, woody, a bit of green
3c	Navajo White; liquid	Popcorn-like, cocoa, buttery, sweet, a bit of green
3d	Peru; Liquid	Weak, roasted, coffee, woody, a bit of oil
3e	Chocolate; Liquid	Toast, waxy, green, a bit of toffee

3a-3c mainly occurred at 270.9–285.6°C with an initial mass reduction of 82.7–85.5%. Following that, the samples demonstrated a steady and homogeneous mass loss trend, and the total weight loss was 98.9–99.6% of their original mass. According to the TG and DTG curves of **3d**, the majority of thermal mass loss (96.08%) occurs between 108.4 °C and 241.2 °C, with a final total weight loss of 97.4%. The decomposition of samples progressed as temperature increases, hence it showed the sample with relatively poor thermal stability and decomposed first at lower decomposition temperatures. It might be attributed to the differences in chemical structures, such as the structure of **3d** having ethoxyl group and the structures of **3a**, **3b** and **3c** having the methoxy group, which resulted in different stabilizations. Furthermore, the decomposition temperatures of **3e** were lower than those of the other samples, which occurred predominantly between 58.7 and 118.7 °C with a weight decrease of 97.29% from the beginning. This can be explained by the fact that the molecular weight of **3e** is lower than that of **3a-3d**, and it starts losing its component by volatilization at lower temperatures than others. The TG-DTG testing revealed that these five samples were stable at room temperature.

The DSC curves for **3a-3e** analyzed in air atmosphere are presented in Fig. 2 (b). The enthalpy change of the samples and the peak temperature of DSC curves were recorded by apparatus. The T_{onset} , T_{peak} , and T_{end} temperatures were comparable to those determined based on DTG curves. In particular, it can be seen that there is a sharp, large endothermic peak at 53.9 °C with the DSC curve of **3a**. On contrary, there is no weight loss at 53.9 °C, indicating that the sharp peak represents a melting-point of **3a**. Moreover, it indicated that the T_{peak} of **3a-3e** in DSC curves happened in main mass loss regions, which indicates that the samples may have vaporized or decomposed during the endothermic phase (Muravyev et al., 2017; Searcy and Beruto, 1976).

In overall, the TG-DTG and DSC data commonly acknowledged with one another and demonstrated the stability of the title compounds at room temperature. The data con-

cerning the results obtained based on those curves which are given in Table 3. It is worth noting that these five compounds have extremely significant enthalpy change values, particularly in compound **3e**. This behavior might be explained by low molecular weight of compound **3e** and obvious absence of a benzene ring structure, which was also consistent with the TG-DTG results.

3.4. Pyrolysis analysis

Although the thermal stability of the samples was satisfactory in TG-DTG and DSC testing, the pyrolysis products were not recognized. Thus, it was also necessary to investigate the components released under heating conditions. The pyrolysis conditions were set at 100–300, 300–900 °C in pure nitrogen and 30–900 °C in an oxidative atmosphere (9% oxygen with 91% nitrogen). Besides, the pyrolysis gas chromatograms obtained at different heating conditions were shown in Fig. 3, and the total ion peak areas of pyrolysis products were summarized in Table 4.

The pyrolysis in pure nitrogen at 100–300 °C culminated in the vaporization of these five samples with no decomposition products, which helps us to determine the thermal stability of **3a-3e** from another viewpoint. However, minimal reaction products were detected after the thermal decomposition of the five samples at higher temperatures. It can be seen that compounds **3a**, **3b**, and **3e** showed an evaporative yield of 86.12–92.26% and 75.01–87.61% during the high-temperature in pure nitrogen and oxidative atmosphere, respectively. The data in Table 3 revealed that the Py products of **3a**, **3b**, and **3e** were composed of two series of derivatives generated from the alkyl pyrazinyl unit and the carboxylic acid unit. The pyrolysis products from the alkyl pyrazinyl unit of **3a**, **3b**, and **3e** were similar in principle, including 2-methylpyrazine, 2,5-dimethylpyrazine, 2-ethylpyrazine, as well as 2-ethyl-5-methylpyrazine, etc. And most of the pyrolysis products from the carboxylic acid unit of compounds **3a**, **3b**, and **3e** were benzyl derivatives such as benzoic acid, and pivalic

Table 3 Thermal analysis data for compounds **3a-3e**.

Sample	TG-DTG analysis				DSC analysis			
	T_i (°C)	T_b (°C)	T_p (°C)	T_p rate (%/ min)	T_{onset} (°C)	T_{Peak} (°C)	T_{end} (°C)	ΔH (kJ/mol)
3a	183.4	290.4	285.6	28.3	276.1	289.7	296.4	113.8
3b	160.9	283.4	270.9	27.2	243.1	277.9	285.6	226.4
3c	163.1	295.4	280.6	29.1	270.2	288.3	284.9	149.6
3d	108.4	241.2	213.7	28.9	189.2	213.2	215.3	57.9
3e	58.7	188.7	148.7	27.8	149.7	158.7	165.3	6.9

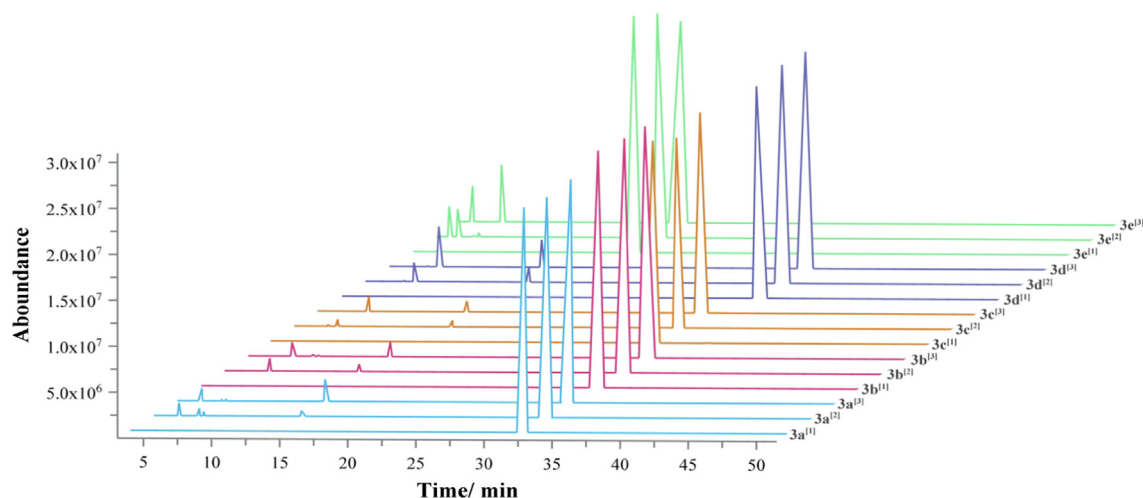


Fig. 3 Pyrolysis of the compounds **3a-3e** in different conditions: [1] 100–300 °C in N₂; [2] 300–900 °C in N₂; [3] 30–900 °C in 9% oxygen and 91% N₂.

Table 4 Pyrolysis products of **3a-3e** (TIC area%).

Sample	Peak No.	Compound	Heating conditions		
			N ₂		9% O ₂ in N ₂
			100–300 °C	300–900 °C	30–900 °C
3a	1	2-Methylpyrazine	–	4.46	4.76
	2	2-Ethylpyrazine	–	2.27	0.56
	3	2-Vinylpyrazine	–	1.17	0.79
	4	Benzoic acid	–	2.61	7.41
	5	Pyrazin-2-ylmethyl benzoate (3a)	100	89.47	86.46
3b	1	2,5-Dimethylpyrazine	–	4.87	5.71
	2	2-Ethyl-5-methylpyrazine	–	–	0.90
	3	2-Methyl-5-vinylpyrazine	–	–	0.62
	4	Benzoic acid	–	2.86	5.14
	5	(5-Methylpyrazin-2-yl)methyl benzoate (3b)	100	92.26	87.61
3c	1	2-Ethylpyrazine	–	0.43	–
	2	2-Vinylpyrazine	–	2.78	6.97
	3	Benzoic acid	–	2.60	4.17
	4	1-(Pyrazin-2-yl)ethyl benzoate (3c)	100	94.17	88.85
3d	1	2-Ethylpyrazine	–	0.06	0.03
	2	2-Vinylpyrazine	–	7.00	11.8
	3	Benzoic acid	–	4.73	8.69
	4	2-(Pyrazin-2-yl)ethyl benzoate (3d)	100	88.85	80.18
3e	1	Pivalic acid	–	6.12	8.58
	2	2-Methylpyrazine	–	5.56	14.69
	3	2-Ethylpyrazine	–	0.68	–
	4	2-Vinylpyrazine	–	1.50	–
	5	Pyrazin-2-ylmethyl pivalate (3e)	100	86.12	75.01

acid. When compared to pure nitrogen, the relative peak regions of methyl-pyrazines were found to be higher in the oxidizing atmosphere. Furthermore, compound **3c** was the most stable substance during the testing, with just 5.83% and 11.14% decomposition at high temperatures in pure nitrogen and oxidative atmospheres, respectively. When the volatile pyrolysis products of **3c** and **3d** were examined, the most abundant byproducts were 2-vinylpyrazine and benzoic acid. And both of their degrees of decomposition were significantly higher in the oxidative atmosphere than in pure nitrogen. Over all, compared to a pure nitrogen atmosphere, the peak areas

for the pyrolyzed products from compounds **3a-3e** were larger in the oxidative atmosphere. For instance, higher quantities of pyrazine products were produced and the proportion of cleavage products such as the corresponding acids increased in the oxidative condition. It might be due to the involvement of O₂ from the mixed atmosphere (9% oxygen with 91% nitrogen) during the heating process, causing the cleavage and oxidation mechanisms to become more complicated and varied (Lai et al., 2017).

It is worth mentioning that the unique flavor compounds were found among the pyrolysis byproducts of the five sam-

ples, including benzoic acid, 2-methylpyrazine, 2,5-dimethylpyrazine, 2-ethylpyrazine, 2-ethyl-5-methylpyrazine, 2-vinylpyrazine, and 2-methyl-5-vinylpyrazine. It can be determined that the pyrolysis analysis of title compounds at low temperature confirmed the stability and uniformity of volatilization under heat treatment. Meanwhile, most of the samples evaporated during the high-temperature treatment, and only a small fraction decomposed endothermically, producing unique characteristic aroma compounds.

3.5. *In vitro* antifungal activity

According to the literature, there are rare relevant reports on the antifungal activities of pyrazine ester derivatives to date. Thus, the antifungal properties of pyrazine esters against *R. solani*, *P. nicotianae*, *F. oxysporum*, *F. graminearum*, and *F. moniliforme* were evaluated in this study by comparing the triazole of 0.03 mg/ml as a positive control. And Fig. 4 shows the findings of their antifungal activities. Careful observation of these results obtained revealed that majority of these title compounds displayed better antifungal effectiveness against five organisms than those of the positive and blank control.

Firstly, we tested the title compounds against *F. oxysporum*, *F. graminearum*, and *F. moniliformes*. The bioassay analysis indicated that **3a-3e** had some antifungal activity to some extent, with an inhibitory index ranging from 13.8 to 78.2%. And it was noteworthy that compound **3c** has higher activity than the other compounds, with an inhibitory index of 78.2%, 64.7%, and 50.5%, respectively. Inspiringly, the activity results against *R. solani* by the compounds **3a-3e** showed excellent inhibitory activity, with an inhibitory index of 82.0–94.3%. Furthermore, all compounds, especially compound **3c**, demonstrated considerable antifungal activity against *P. nicotianae* with an inhibitory index of 46.1–81.8%.

Based on the results of the above analysis, we selected several compounds with excellent antifungal activity (inhibitory index > 80%) at 0.5 mg/ml to determine the EC₅₀ value

(Fig. 5). As shown in Table 5, it can be concluded that **3c** was the most effective against *R. solani* and *P. nicotianae* with the EC₅₀ value of 0.0191 mg/ml and 0.1870 mg/ml. Moreover, compounds **3a** and **3b** also showed promising antifungal activity against *R. solani* with an EC₅₀ value of 0.0209 mg/ml and 0.0218 mg/ml, respectively. In overall, these results led us to believe that these compounds showed great inhibitory effects on fungus, having the potential to be used for medical and agricultural purposes.

3.6. Molecular docking

To preliminarily explore the possible antifungal mechanism of synthesized target compounds, we performed the molecular docking of highly fungicidal activity compounds **3c** with SDH protein (Q9UTJ7). To make the docking model more clear, only major interactions were highlighted. Generally, the ligand and receptor protein can bind spontaneously when the negative binding energy of the ligand and target protein is greater than zero (Li et al., 2020). The negative binding energy value of compound **3c** with the target protein was -8.3 kcal/mol, preliminarily indicating that compound **3c** has a high affinity for the target protein.

As shown in Fig. 6, compound **3c** was embedded in the active pocket of SDH protein via the connection of hydrogen-bonding, salt bridge, and hydrophobic interactions with some crucial amino acid residues. For example, the compound **3c** may bind to the receptor protein's amino acid residues at positions 92 (HIS 92) and 63 (GLY 63) through two hydrogen bonds of 3.0 Å and 4.1 Å, respectively. And it was linked to the LYS amino acid residue at position 85 of the receptor protein by two hydrogen bonds of 3.9 Å and 3.5 Å, as well as a salt bridge of 4.5 Å. Moreover, it interacted with the receptor protein's ALA amino acid residue at position 214 (ALA214), VAL amino acid residue at position 60 (VAL60), THR amino acid residue at position 249 (THR249), and LEU amino acid residue at position 86

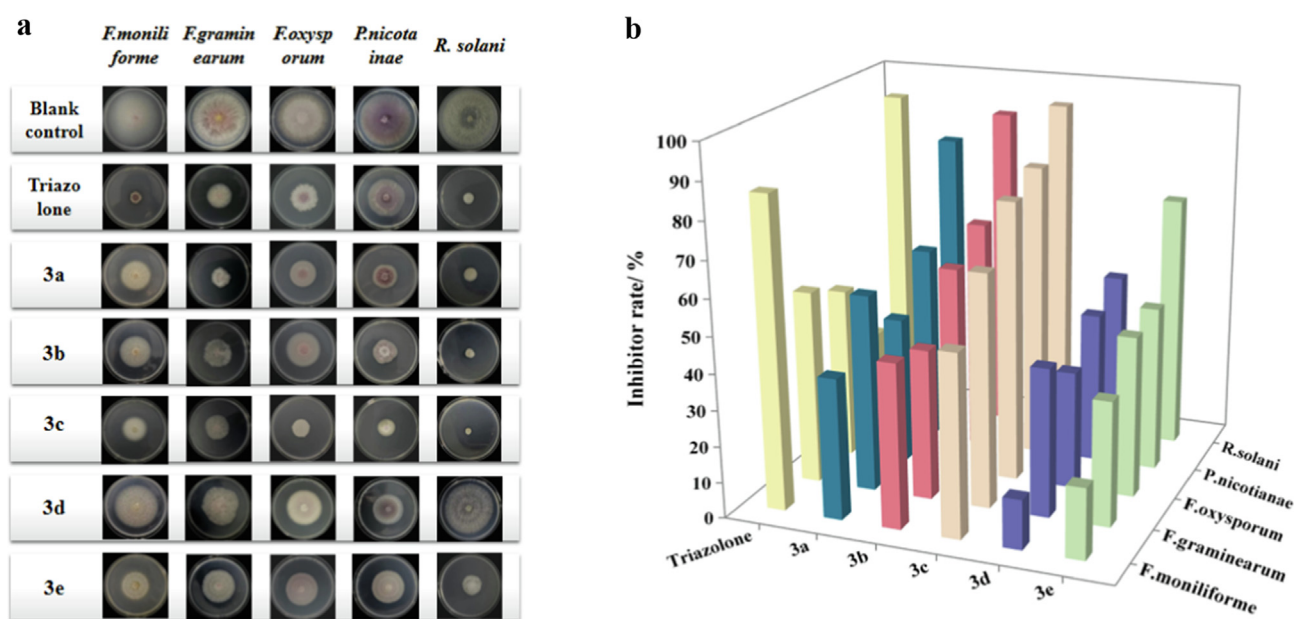


Fig. 4 Antifungal activity of **3a-3e** at 0.5 mg/ml.

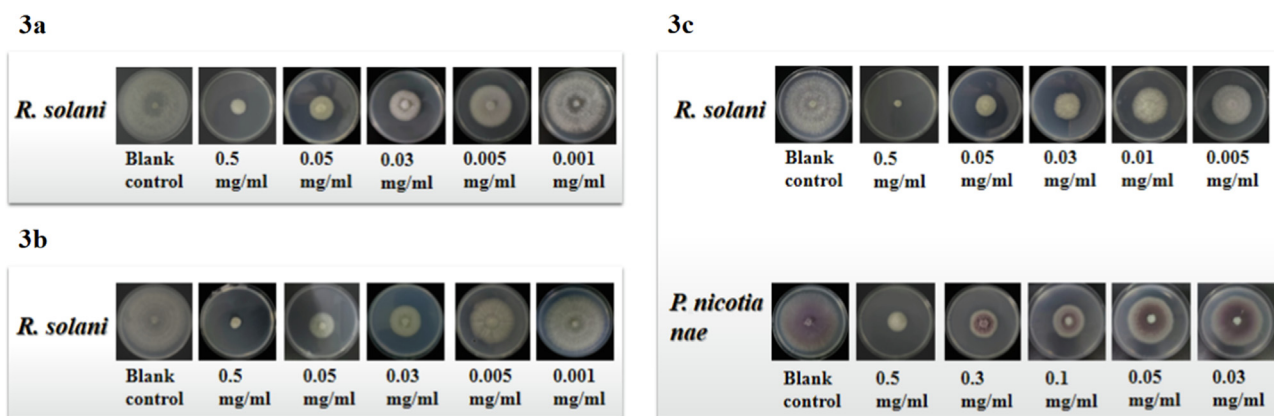


Fig. 5 Antifungal activity of selected compounds.

Table 5 Antifungi potency (EC_{50}) of selected compounds.

Fungi.	Compound	$\lg EC_{50}$		EC_{50} (mg/ ml)
		Regression equation	R^2	
<i>R. solani</i>	3a	$y = 22.973x + 88.599$	0.9964	0.0209
	3b	$y = 29.685x + 99.332$	0.9952	0.0218
	3c	$y = 28.683x + 99.282$	0.9946	0.0191
<i>P. nicotiana</i>	3c	$y = 60.407x + 93.983$	0.9901	0.1870

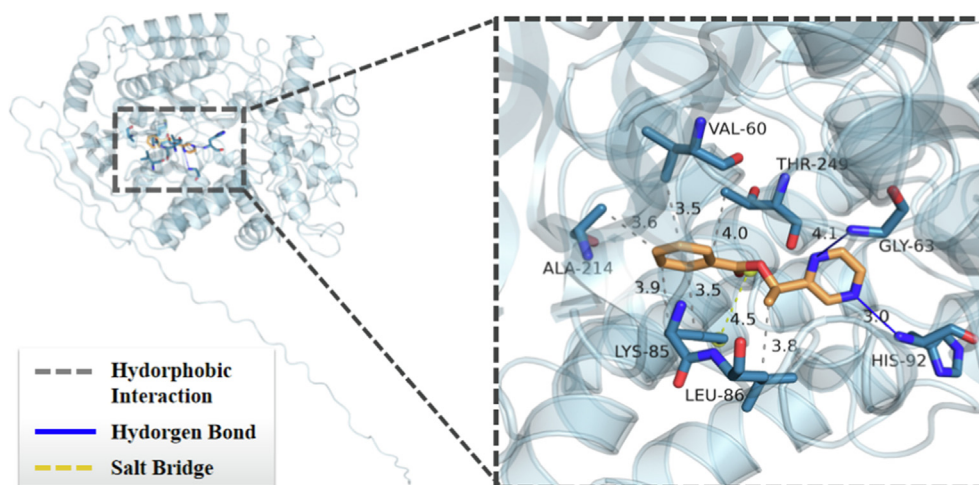


Fig. 6 The binding mode of 3c with target protein.

(LEU86) via four hydrophobic interactions of 3.6 Å, 3.5 Å, 4.0 Å, and 3.8 Å, respectively. All of these favorable interactions may result in the great fungicidal activity of compound 3c.

4. Conclusion

In summary, we developed an effective metal-free esterification method based on pyrazinyl methanol with acid chloride derivatives for the synthesis of five pyrazine esters, and the characterization of their structure (NMR, IR, HRMS) and organoleptic properties were identified. The thermal properties of compounds 3a-3e were investigated using TG, DTG, DSC and Py-GCMS techniques. The TG and DTG measure-

ments revealed that compounds 3a, 3b, and 3c had comparable thermal stability, as evidenced by the total mass loss of 82.7–85.5% from the beginning which occurred primarily at temperatures ranging between 160.9 and 285.6 °C. Due to the instability of 3d by its ethanol-based structure, the thermal mass loss occurred mostly in the temperature ranging from 108.4 to 241.2 °C with a mass loss of 96.08% at the final stages. The thermal mass loss of 3e occurred largely at temperatures ranging from 58.7 to 118.7 °C with a mass loss of 97.29% of the total mass, released component at lower temperatures than others because of its smaller molecular. The T_{peak} of 3a-3e in DSC curves appeared at main mass loss areas, confirming either vaporization or decomposition of the samples occurred during the endothermic phase. The Py-GC/MS results indicated that all compounds volatilize at low-temperature (100–300 °C) in the pure nitrogen atmosphere.

Compounds **3a-3e** were also volatilized under high temperature conditions with yields of 86.12%-92.26% (pure nitrogen) and 75.01%-88.85% (9% oxygen), producing a range of aromatic and natural substances such as 2-methylpyrazine, 2,5-dimethylpyrazine, 2-ethylpyrazine, 2-ethyl-5-methylpyrazine, 2-vinylpyrazine, 2-methyl-5-vinylpyrazine and benzoic acid. And **3c** showed the best thermal stability of all compounds, with only 5.83% and 11.14% decomposition were detected under the high-temperature heating in pure nitrogen and oxidative atmosphere, respectively. Furthermore, the *in vitro* antifungal tests indicated that all compounds exhibited inhibitory effectiveness. For instance, compound **3c** showed the greatest activities of 94% and 80% at 0.5 mg/ml in inhibiting both *R. solani* and *P. nicotianae* with the EC₅₀ values of 0.0191 mg/ml and 0.1870 mg/ml, respectively. Compounds **3a** and **3b** also exhibited effective inhibitor rates of 82% and 91% at 0.5 mg/ml against *R. solani* with the EC₅₀ values of 0.0209 mg/ml and 0.0218 mg/ml, respectively. The result of molecular docking showed that the favorable interactions between compound **3c** and SDH may result in the potent fungicidal activity of compound **3c**. Further studies on the uses of pyrazine esters in the field of flavors and agricultural products are being conducted in our laboratory.

Declaration of Competing Interest

The authors declare that they have no known competing financial interests or personal relationships that could have appeared to influence the work reported in this paper.

Acknowledgments

We were supported by the Key Science and Technology Program of Science and Technology Department of Henan Province [132102210042] and Henan Agricultural University [30500845].

References

- Adams, T.B., Doull, J., Feron, V.J., Goodman, J.L., Marnett, L.J., Munro, L.C., Newberne, P.M., Portoghesi, P.S., Smith, R.L., Waddell, W.J., Wagner, B.M., 2002. The FEMA GRAS assessment of pyrazine derivatives used as flavor ingredients. *Food Chem. Toxicol.* 40, 429–451. [https://doi.org/10.1016/S0278-6915\(01\)00123-5](https://doi.org/10.1016/S0278-6915(01)00123-5).
- Al-Hazmy, S.M., Babaqi, A.S., Daltrozzo, K., M., Sauterb, J., Ebeidc, EM., 1999. A new diolefinic laser dye: 2, 5-bis-2-(2-naphthyl) vinyl pyrazine (B2NVP). *J. Photoch. Photobio. A.* 122, 17–22. [https://doi.org/10.1016/S1010-6030\(98\)00435-3](https://doi.org/10.1016/S1010-6030(98)00435-3).
- Amrani-Hemaimi, M., Cerny, C., Fay, L.B., 1995. Mechanisms of formation of alkylpyrazines in the Maillard reaction. *J. Agric. Food Chem.* 43, 2818–2822. <https://doi.org/10.1021/jf00059a009>.
- Asaki, T., Hamamoto, T., Sugiyama, Y., Kuwano, K., Kuwabara, K., 2007. Structure-activity studies on diphenylpyrazine derivatives: A novel class of prostacyclin receptor agonists. *Bioorgan. Med. Chem.* 15, 6692–6704. <https://doi.org/10.1016/j.bmc.2007.08.010>.
- Bao, J.P., Xu, C.L., Yang, G.Y., Wang, C.X., Zheng, X., Yuan, X.X., 2019. Novel 6a, 12b-Dihydro-6 H, 7 H-chromeno [3, 4-c] chromen-6-ones: Synthesis. Structure and antifungal activity. *Molecules.* 24, 1745. <https://doi.org/10.3390/molecules24091745>.
- Bohman, B., Jeffares, L., Flematti, G., Byrne, L.T., Skelton, B.W., Phillips, R.D., 2012. Discovery of tetrasubstituted pyrazines as semiochemicals in a sexually deceptive orchid. *J. Nat. Prod.* 75, 1589–1594. <https://doi.org/10.1021/np300388y>.
- Bonde, C.G., Gaikwad, N.J., 2004. Synthesis and preliminary evaluation of some pyrazine containing thiazolines and thiazolidinones as antimicrobial agents. *Bioorgan. Med. Chem.* 12, 2151–2161. <https://doi.org/10.1016/j.bmc.2004.02.024>.
- Chen, X., Liu, M., Liu, Y., Chen, Y., Au, C.T., Yin, S.-F., 2018. Copper catalyzed esterification of *N*-Heteroaryl methanes by oxidative dehydrogenation. *Asian J. Org. Chem.* 7, 1825–1829. <https://doi.org/10.1002/ajoc.201800421>.
- Chen, Z., Wen, X., Zheng, W., He, R., Chen, D., Cao, D., Ye, M., 2020. Acyl cyanides as bifunctional reagent: application in copper-catalyzed cyanoamidation and cyanoesterification reaction. *J. Org. Chem.* 85, 5691–5701. <https://doi.org/10.1021/acs.joc.9b03500>.
- Cheng, L., Sun, Y., Wang, W., Yao, C., Li, T.J., et al, 2019. Ligand-free copper (I)-catalyzed benzylic acyloxylation of 2-alkylpyridines under aerobic conditions. *J. Org. Chem.* 84, 3074–3082. <https://doi.org/10.1021/acs.joc.8b02794>.
- Chylewska, A., Biedulska, M., Głębocka, A., Raczynska, E.D., Makowski, M., 2019. Drug-like properties and complete physico-chemical profile of pyrazine-2-amidoxime: A combined multi-experimental and computational studies. *J. Mol. Liq.* 276, 453–470. <https://doi.org/10.1016/j.molliq.2018.11.147>.
- Czégény, Z., Bozi, J., Sebestyén, Z., Blazsó, M., Jakab, E., Barta-Rajnai, E., Liu, C., 2016. Thermal behaviour of selected flavour ingredients and additives under simulated cigarette combustion and tobacco heating conditions. *J. Anal. Appl. Pyrol.* 121, 190–204. <https://doi.org/10.1016/j.jaap.2016.07.020>.
- da Silva, Y.K.C., Augusto, C.V., de Castro Barbosa, M.L., de Albuquerque Melo, G.M., de Queiroz, A.C., 2010. Synthesis and pharmacological evaluation of pyrazine *N*-acylhydrazone derivatives designed as novel analgesic and anti-inflammatory drug candidates. *Bio. Med. Chem.* 18, 5007–5015. <https://doi.org/10.1016/j.bmc.2010.06.002>.
- Dolezal, M., Zitko, J., 2015. Pyrazine derivatives: a patent review (June 2012-present). *Expert opin. Ther. pat.* 25, 33–47. <https://doi.org/10.1517/13543776.2014.982533>.
- Eisele, P., Bauder, M., Hsu, S.F., Plietker, B., 2019. A cyanide-free synthesis of acylcyanides through Ru-catalyzed C (sp³)-H-oxidation of benzylic nitriles. *Chemistry Open.* 8, 689–691. <https://doi.org/10.1002/open.201900130>.
- Fales, H.M., Blums, M.S., Southwick, E.W., William, D.L., Roller, P. P., Don, A.W., 1988. Structure and synthesis of tetrasubstituted pyrazines in ants in the genus mesoponera. *Tetrahedron.* 44, 5045–5050. [https://doi.org/10.1016/S0040-4020\(01\)86009-9](https://doi.org/10.1016/S0040-4020(01)86009-9).
- Gonzalez, M., Pujol, M., METRAUX, J. P., GONZALEZ-GARCIA, V., Bolton, M. D., BORRÁS-HIDALGO, O., 2011. Tobacco leaf spot and root rot caused by *Rhizoctonia solani* Kühn. *Mol. Plant pathol.* 12, 209–216. <https://doi.org/10.1111/j.1364-3703.2010.00664.x>.
- Harries, E., Berruezo, L.A., Galván, M.Z., Rajal, V.B., Mercado Cárdenas, G.E., 2020. Soil properties related to suppression of *Rhizoctonia solani* on tobacco fields from northwest Argentina. *Plant Pathol.* 69, 77–86. <https://doi.org/10.1111/ppa.13106>.
- Huang, X., Li, X., Zou, M., Song, S., Tang, C., Yuan, Y., Jiao, N., 2014. From ketones to esters by a Cu-catalyzed highly selective C (CO)-C (alkyl) bond cleavage: aerobic oxidation and oxygenation with air. *J. Am. Chem. Soc.* 136, 14858–14865. <https://doi.org/10.1021/ja5073004>.
- Jaiswal, Y., Kumar, Y., Pal, J., Subramanian, R., Kumar, A., 2018. Rapid synthesis of polysubstituted phenanthridines from simple aliphatic/aromatic nitriles and iodo arenes via Pd (II) catalyzed domino C-C/C-C/C-N bond formation. *Chem. Commun.* 54, 7207–7210. <https://doi.org/10.1039/C8CC03556C>.
- Juhás, M., Zitko, J., 2020. Molecular interactions of pyrazine-based compounds to proteins. *J. Med. Chem.* 63, 8901–8916. <https://doi.org/10.1021/acs.jmedchem.9b02021>.
- Koehler, P.E., Mason, M.E., Odell, G.V., 1971. Odor threshold levels of pyrazine compounds and assessment of their role in the flavor of roasted foods. *J. Food Sci.* 36, 816–818. <https://doi.org/10.1111/j.1365-2621.1971.tb03314.x>.
- Koehler, P.E., Odell, G.V., 1970. Factors affecting the formation of pyrazine compounds in sugar-amine reactions. *J. Agric. Food Chem.* 18, 895–898. <https://doi.org/10.1021/jf60171a041>.

- Kosuge, T., Kamiya, H., 1962. Discovery of a pyrazine in a natural product: tetramethylpyrazine from cultures of a strain of *Bacillus subtilis*. *Nature*. 193, 776–776. <https://doi.org/10.1038/193776a0>.
- Krems, I.J., Spoerri, P.E., 1947. The pyrazines. *Chem. Rev.* 40, 279–358. <https://doi.org/10.1021/cr60126a004>.
- Kucerova-Chlupacova, M., Kunes, J., Buchta, V., Vejsova, M., Opletalova, V., et al., 2015. Novel pyrazine analogs of chalcones: synthesis and evaluation of their antifungal and antimycobacterial activity. *Molecules*. 20, 1104–1117. <https://doi.org/10.3390/molecules20011104>.
- Lai, M., Ji, X.M., Tao, T., Shan, Y.Y., Liu, P.F., Zhao, M.Q., 2017. Synthesis and pyrolysis of two flavor precursors of oct-1-en-3-yl methylpyrazinecarboxylates. *J. Therm. Anal. Calorim.* 128, 1627–1638. <https://doi.org/10.1007/s10973-016-6083-5>.
- Lee, J.Y., Aoyama, T., Uchiyama, M., 2020. Synthesis and properties of liquid pyrazine dyes. *Dyes pigments*. 174. <https://doi.org/10.1016/j.dyepig.2019.108030> 108030.
- Lee, E.S., Kim, N., Kang, J.H., Abdildinova, A., Lee, S.H., Lee, M.H., Kang, N.S., Koo, T.S., Kim, S.Y., Gong, Y.D., 2022. Design and synthesis of a novel 4-aryl-N-(2-alkoxythieno [2,3-b] pyrazine-3-yl) -4-arylpiperazine-1-carboxamide DGG200064 showed therapeutic effect on colon cancer through G2/M arrest. *Pharmaceuticals*. 15, 502. <https://doi.org/10.3390/ph15050502>.
- Li, H., Gao, M. Q., Chen, Y., Wang, Y. X., Zhu, X. L., Yang, G. F., 2020. Discovery of pyrazine-carboxamide-diphenyl-ethers as novel succinate dehydrogenase inhibitors via fragment recombination. *J. Agri. Food Chem.* 68, 14001–14008. <https://doi.org/10.1021/acs.jafc.0c05646>.
- Maga, J.A., Katz, I., 1982. Pyrazines in foods: an update. *Crit. Rev. Food Sci.* 16, 1–48. <https://doi.org/10.1080/10408398209527323>.
- Maga, J.A., Sizer, C.E., Myhre, D.V., 1973. Pyrazines in foods. *Crit. Rev. Food Sci.* 4, 39–115. <https://doi.org/10.1080/10408397309527153>.
- Masuda, H., Yoshida, M., Shibamoto, T., 1981. Synthesis of new pyrazines for flavor use. *J. Agr. Food Chem.* 29, 944–947. <https://doi.org/10.1021/jf00107a014>.
- Michael, Z., Abushqara, E., Hodrien, D., 2005. Chocarom pyrazine: A remarkable pyrazine for flavors and fragrances. 13, 189–202. <https://doi.org/10.1021/bk-2005-0908.ch013>.
- Mihara, S., Masuda, H., 1988. Structure-odor relationships for disubstituted pyrazines. *J. Agr. Food Chem.* 36, 1242–1247. <https://doi.org/10.1021/jf00084a029>.
- Minjiyar, P.B., Murumkar, P.R., Patil, P.S., Barmade, A., M., G Bothara, K., 2013. Unequivocal role of pyrazine ring in medicinally important compounds: A review. *Mini Reviews in Medicinal Chemistry* 13, 1607–1625.
- Mortzfeld, F.B., Hashem, C., Vranková, K., Winkler, M., Rudroff, F., 2020. Pyrazines: Synthesis and industrial application of these valuable flavor and fragrance compounds. *Biotechnol. J.* 15, 2000064. <https://doi.org/10.1002/biot.202000064>.
- Muravyev, N.V., Koga, N., Meerov, D.B., Pivkina, A.N., 2017. Kinetic analysis of overlapping multistep thermal decomposition comprising exothermic and endothermic processes: thermolysis of ammonium dinitramide. *Phys. Chem. Chem. Phys.* 19, 3254–3264. <https://doi.org/10.1039/C6CP08218A>.
- Murillo, I., Cavallarin, L., San-Segundo, B., 1998. The development of a rapid PCR assay for detection of *Fusarium moniliforme*. *Eur. J. of Plant Pathol.* 104, 301–311. <https://doi.org/10.1023/A:1008698919376>.
- Nelson, P.E., 1992. Taxonomy and biology of *Fusarium moniliforme*. *Mycopathologia*. 117, 29–36. <https://doi.org/10.1007/BF00497276>.
- Ntushelo, K., 2016. Chlorinated organic compounds produced by *Fusarium graminearum*. *Acta Biol. Hung.* 67, 220–224. <https://doi.org/10.1556/018.67.2016.2.10>.
- Oldham, N.J., Morgan, E.D., 1993. Structures of the pyrazines from the mandibular gland secretion of the ponerine ant *dinoponera australis*. *J. Chem. Soc. Perkin Trans. 1*, 2713–2716. <https://doi.org/10.1039/P19930002713>.
- Peng, P., Linseis, M., Winter, R.F., Schmidt, R.R., 2016. Regioselective acylation of diols and triols: the cyanide effect. *J. Am. Chem. Soc.* 138, 6002–6009. <https://doi.org/10.1021/jacs.6b02454>.
- Prasad, A.K., Kumar, V., Maity, J., Wang, Z., Ravikumar, V.T., Sanghvi, Y.S., Parmar, V.S., 2005. Benzoyl cyanide: a mild and efficient reagent for benzylation of nucleosides. *Synthetic commun.* 35, 935–945. <https://doi.org/10.1081/SCC-200051693>.
- Rolver, M.G., Elingaard-Larsen, L.O., Andersen, A.P., Counillon, L., Pedersen, S. F., 2020. Pyrazine ring-based Na⁺/H⁺ exchanger (NHE) inhibitors potently inhibit cancer cell growth in 3D culture, independent of NHE1. *Sci. Rep. UK* 10, 1–17. <https://doi.org/10.1038/s41598-020-62430-z>.
- Searcy, A.W., Beruto, D., 1976. Kinetics of endothermic decomposition reactions. I. Steady-state chemical steps. *J. Phys. Chem. C*. 80, 425–429. <https://doi.org/10.1021/j100545a017>.
- Seitz, L.E., Suling, W.J., Reynolds, R.C., 2002. Synthesis and antimycobacterial activity of pyrazine and quinoxaline derivatives. *J. Med. Chem.* 45, 5604–5606. <https://doi.org/10.1021/jm020310n>.
- Seliem, I.A., Girgis, A.S., Moatasim, Y., Kandeil, A., Mostafa, A., Ali, M.A., Bekheit, M.S., Panda, S.S., 2021. New pyrazine conjugates: synthesis, computational studies, and antiviral properties against SARS-CoV-2. *Chem. Med. Chem.* 16, 3418–3427. <https://doi.org/10.1002/cmdc.202100476>.
- Tambat, N., Mulani, S.K., Ahmad, A., Shaikh, S.B., Ahmed, K., 2022. Pyrazine derivatives-versatile scaffold. *Russ. J. Bioorg. Chem.* 9, 1–31. <https://doi.org/10.1134/S1068162022050259>.
- Wagner, R., Czerny, M., Bielohradsky, J., Grosch, W., 1999. Structure odour-activity relationships of alkylpyrazines. *Z. Lebensm. Unters. Forsch.* 208, 308–316. <https://doi.org/10.1007/s002170050422>.
- Wang, Z., Zeng, G., Wei, X., Ding, B., Huang, C., Xu, B., 2016. Determination of vanillin and ethyl-vanillin in milk powder by headspace solid-phase microextraction coupled with gas chromatography-mass spectrometry. *Food Anal. Method.* 9, 3360–3366. <https://doi.org/10.1007/s12161-016-0520-8>.
- Xie, W., Tang, J., Gu, X., Luo, C.R., Wang, G.Y., 2007. Thermal decomposition study of menthyl-glycoside by TGA/SDTA, DSC and simultaneous Py-GC-MS analysis. *J. Anal. Appl. Pyrol.* 78, 180–184. <https://doi.org/10.1016/j.jaap.2006.06.007>.
- Yang, G., Shi, L., Pan, Z., Wu, L., Fan, L., Wang, C., Liang, J., 2021. The synthesis of coumarin thiazoles containing a trifluoromethyl group and their antifungal activities. *Arab. J. Chem.* 14. <https://doi.org/10.1016/j.arabjc.2020.10.027> 102880.
- Yang, J.K., Tong, Z.J., Fang, D.H., Chen, X.J., Zhang, K.Q., Xiao, B. G., 2017. Transcriptomic profile of tobacco in response to *Phytophthora nicotianae* infection. *Scientific Rep.-UK* 7, 1–7. <https://doi.org/10.1038/s41598-017-00481-5>.
- Zhu, J., Wu, Y., Xu, L., Jin, J., 2020. Theoretical studies on the selectivity mechanisms of glycogen synthase kinase 3 β (GSK3 β) with pyrazine ATP-competitive inhibitors by 3D-QSAR, molecular docking, molecular dynamics simulation and free energy calculations. *Curr. Comput. -Aid. Drug.* 16, 17–30. <https://doi.org/10.2174/1573409915666190708102459>.